The Complementary Nature of X-Ray Photoelectron Spectroscopy and Angle-Resolved X-Ray Diffraction Part II: Analysis of Oxides on Dental Alloys

S.J. Kerber, T.L. Barr, G.P. Mann, W.A. Brantley, E. Papazoglou, and J.C. Mitchell

(Submitted 12 February 1998)

X-ray photoelectron spectroscopy (XPS) and angle-resolved x-ray diffraction (ARXRD) were used to analyze the oxide layer on three palladium-gallium-based dental casting alloys. The oxide layers were approximately 10 μm thick. The use of the techniques helped to determine which mechanism was responsible for oxide formation—either (a) oxide layer growth via diffusion of oxygen through the scale to the metal, causing the scale to grow at the metal-oxide interface, or (b) an oxide layer formed by metal ions diffusing through the scale to the surface and reacting with oxygen, causing the scale to grow at the oxide-air interface. The oxide growth mechanisms were correlated to previous layer adhesion results determined with biaxial flexure testing.

Keywords angle resolved, dental alloys, gallium, oxide, palladium, review, x-ray diffraction, x-ray photoelectron spectroscopy

1. Introduction

Both x-ray diffraction (XRD) and x-ray photoelectron spectroscopy (XPS, also known as ESCA, electron spectroscopy for chemical analysis) are commonly used to analyze oxide layers (Ref 1-6). In theory, XRD identifies crystalline materials within (approximately) the top 10 μm of a surface. The expanded technique of angle-resolved x-ray diffraction (ARXRD) utilizes a fixed x-ray source with a scanning detector; in the scientific literature this technique is generally termed grazing-angle x-ray diffraction (Ref 7-12). If the source is set at a very shallow glancing angle, the x-rays detected are from a near surface region of a few tens of nanometers. As the incident angle increases and moves closer to normal to the surface, the signal is obtained from an increasing depth of the material. In this study, the x-ray source was varied from grazing values of <1° to incident angles of 20°, which can no longer be defined as grazing. The ARXRD terminology was chosen because of its correspondence to the use of angle-resolved XPS for depth profiling of surface layers (2 to 8 nm) (Ref 13). When XPS (which typically analyzes a depth of 5 nm) is combined with argon ion depth profiling, chemical information as a function of depth is also obtained, typically to maximum depths of a few hundred nanometers. In practice, the analysis of complex oxides with either of these techniques can be complicated. However, a combination of the two techniques can be used to minimize shortcomings of the individual methods if the backgrounds of the procedures are fully understood and the merging of the data is done with caution. A full discussion of the background and theory of these techniques is included in Part I of this report (Ref 14).

The complex near-surface oxides and metals of three palladium-gallium-based dental alloys were studied. Although high-palladium dental alloys containing greater than ~75 wt% Pd have become popular for metal-ceramic restorations over the past decade because of their lower cost than gold alloys and their good mechanical properties (Ref 15, 16), only limited information is available about their oxidation behavior (Ref 17, 18). After the initial oxidation reported here, dental porcelain is ultimately bonded to the surfaces. The metal/oxide/dental porcelain systems were previously subjected to biaxial flexure tests to determine the relative adhesion of the porcelain (Ref 19). An analysis was conducted in an attempt to correlate the previous porcelain adherence results for the various alloys to the surface oxides present before porcelain bonding. Additionally, the determination of the surface chemistry of the oxide layers may provide guidance in the development of new high-palladium alloys with improved metal-ceramic bonding. A detailed study on the oxides was conducted, combining depth profile XPS and ARXRD. A preliminary account of this work for one alloy has been presented (Ref 20), and full analyses of these alloys and their ramifications on the dental community will be published in separate reports.

2. Experimental

2.1 Alloy Preparation

Three Pd-Ga based dental alloys were selected. Compositions of the alloys are listed in Table 1. The Spartan Plus alloy (Williams/Ivoclar, Amherst, NY) is generally classified as a

S.J. Kerber, Material Interface, Inc., N73W22301 Willowview Drive, Sussex, WI 53089-2244, e-mail: matlinter@aol.com; **T.L. Barr** and **G.P. Mann,** Department of Materials, Laboratory for Surface Studies, University of Wisconsin-Milwaukee, Milwaukee, WI, 53201; e-mail: terybarr@csd.uwm.edu; **W.A. Brantley** and **E. Papazoglou,** Section of Restorative Dentistry, Prosthodontics and Endodontics, College of Dentistry, The Ohio State University, Columbus, OH 43210-1241, e-mail: brantley.1@osu.edu, papazoglou.1@osu.edu; **J.C. Mitchell,** Microscopic and Chemical Analysis Research Center, Department of Geological Sciences, The Ohio State University, Columbus, OH 43210-1308, e-mail: mitchell.3@osu.edu.

Pd-Cu-Ga alloy. The Protocol alloy (Williams/Ivoclar) and the Legacy alloy (Jelenko, Armonk, NY) are classified as Pd-Ga alloys (Ref 15). After casting, oxidating, and subsequent bonding of dental porcelain, metal ceramic samples were loaded to failure in biaxial flexure, and the adhesion of the porcelain was measured by a standardized x-ray spectrometric technique (Ref 19). The Protocol system exhibited a combination of adhesive fracture through the metal-metal oxide interface and cohesive fracture in the porcelain, whereas the Legacy system exhibited substantial or complete fracture through the metal-oxide interface. In contrast, the Spartan Plus system displayed a combination of cohesive failure in the porcelain and adhesive failure between the porcelain and the oxide. Therefore, the initial oxide grown on the surface of the Spartan Plus alloys remained intact, while the oxides on the Protocol and Legacy alloys delaminated.

To determine the reason for the differences in these failure mechanisms, oxidized specimens were prepared of each alloy. Cast specimens of 10 mm by 10 mm by 1 mm were air abraded with alumina, following standard dental laboratory practice and subjected to the oxidation procedures recommended by the alloy manufacturers. Although the cast alloy specimens could have been metallographically polished and etched, rather than air abraded, prior to oxidation, previous research (Ref 18) has shown that this surface treatment causes different oxides to form. The two Williams/Ivoclar alloys (Spartan Plus and Protocol) were oxidized by heating in a mild vacuum (0.95 atm) in a conventional dental porcelain furnace from 650 to 1,010 °C at a rate of 56 °C/min with a 5 min hold at the peak temperature. The Jelenko alloy, Legacy, was oxidized by heating in air from 704 to 1,010 °C at 56 °C/min with no hold at the peak temperature. Scanning electron microscopy (SEM) and microstructural evaluation of these materials has been previously published (Ref 15, 16, 21).

2.2 XPS Analysis

The XPS system used for the analysis was a Hewlett Packard Model 5950A (Palo Alto, CA) with monochromatic aluminum *K*α radiation. The area of analysis was approximately 5 mm by 1 mm. The samples were analyzed in their as-received state and after 1, 3, 7, 15, 25, 100, 200, and 300 min of argon ion depth profiling. The argon ion (Ar^+) energy was approximately 2500 eV. Under these conditions, the sputtering rate for the system was 0.7 nm/min, calibrated to a SiO_2 sputtering standard. Therefore, the depth profile provided detailed information about a surface layer approximately 210 nm in depth.

Table 1 Nominal weight percent compositions (manufacturer supplied) of the high-palladium alloys studied

Alloy	Palladium	Copper	Gallium	Gold	Silver	Indium
Spartan Plus(a)	79	10	9	2	…	…
Protocol(a)	75	…	6	6	6.5	6
Legacy(b)	85	…	10	2	1	1

(a) Williams/Ivoclar, Amherst, NY. (b) J.F. Jelenko & Company, Armonk, NY

Table 2 Peak areas (arbitrary units) as a function of glancing angle for oxidized Spartan Plus alloy

			ARXRD method, incident angle				Standard XRD
	ICDD file no.	Peak location, 2θ	0.75°	1.5°	5°	20°	method
Pd	5-681	40.1	891	2 082	8 171	36 047	83 049
Presumed nonequilibrium form of hydrated palladium oxide	…	34.6	265	528	1 736	4 218	8 253
$PdO{\cdot}xH_2O$	9-254	34.1	57	254	504	1 410	2 523
$CuGa_2O_4$	26-514	35.9	44	147	835	2 784	5 159
Cu_2O	5-667	36.4	54	168	271	755	2 775
βGa_2O_3	43-1012	35.2	0	12	18	72	124

Table 3 Elemental concentration (at.%) obtained by XPS as a function of sputtering time for oxidized Spartan Plus alloy

Argon ion sputtering time, min	C 1s	O 1s	Cu LMM	Ga $2p_3$	Pd $3d_{5/2}$	Au $4f_{7/2}$
0	35.9	49.3	4.3	7.4	3.1	…
1	16.5	52.8	14.8	12.6	3.3	…
3	11.6	52.5	16.5	14.5	4.9	…
7	9.4	49.7	16.5	17.4	7.0	…
15	6.7	51.7	15.3	17.2	8.9	0.1
25	7.4	51.4	13.6	17.7	9.8	0.1
100	6.3	57.4	9.5	13.0	13.4	0.3
200	10.4	45.3	9.9	11.9	22.1	0.4
300	14.7	44.4	8.6	9.7	22.1	0.5

The XPS analysis included survey scans to determine the elemental composition at each depth as well as high-energy resolution scans of each element detected at each depth. The high-energy resolution scans are performed to determine the binding energy of the species detected. From the binding energies, inferences of the compounds present were made via comparison with literature standards (Ref 14). Because the analysis of insulating materials with XPS can cause peak charging shifts, the binding energy values were calibrated to metallic palladium (the clearest and most unambiguous peak in this series) at 335.5 eV. With this palladium calibration, the adventitious carbon peak occurred at 284.6 eV. The XPS binding energies were compared to literature values (Ref 22-27). Quantitative analysis of the data was accomplished with the use of sensitivity factors of Wagner (Ref 27).

2.3 ARXRD Analysis

All data were collected with a Scintag Model 2000 XRD system (Scintag, Inc., Cupertino, CA) using copper *K*α radiation with a solid state analysis filter. The grazing incidence attachment consisted of an exit slit with 0.3° divergence. The step size was 0.1° with step times of 3, 9, or 18 s/step. The x-ray angles of incidence were set at 0.75° (18 s/step), 1.5° (18 s/step), 5° (9 s/step), and 20° (3 s/step). Because the source is fixed, the geometry of the system constrains the 2θ range to 20 to 50 °. The data were compared to International Center for Diffraction Data (ICDD, formerly Joint Committee on Powder Diffraction Standards, Swarthmore, PA) standards that are part of the computer data handling system. For comparison to the angle-resolved data, XRD in the traditional mode was also accomplished on each of the alloys; full results on the standard XRD analysis of the oxidized alloys were published in Ref 18.

Calculations for the 1/e analysis depth (Ref 14) were accomplished using the absorption coefficient for palladium metal (subsequent results show that the major component of the surface layer of the coatings is palladium metal). Attempts were then made to correlate the XPS results with the angle-resolved XRD data. The XRD incident angle of 0.75° was calculated to correspond to a depth of approximately 50 nm. This correspondence correlated to an argon sputtering time (during XPS analysis) of 75 min. The 1.5° incident angle corresponded to 100 nm and a sputtering time of approximately 150 min. The 5° incident angle corresponded to 300 nm or an extrapolated sputtering time of 425 min. An XRD incident angle of 20° was calculated to have a 1/e depth of 700 nm.

Rather than discrete depths, the ARXRD 1/e depths are volume depths and include information from the surface to that depth, and even somewhat beyond. Surface roughness of these samples and differential sputtering complicates the depth measurements obtained from XPS. However, despite their shortcomings, the two techniques, under these experimental conditions, yielded dovetailed information about the surface and near surface composition of the oxide layer (Ref 14).

To summarize, each oxidized alloy was analyzed with XPS. The elemental concentration as a function of sputtering time was obtained. Each element was studied in high-energy resolution mode at each depth to obtain the binding energy of the elements detected and make inferences as to the chemical species present. The XPS experiments yielded information about the outer approximately 210 nm. In parallel, each oxidized alloy was studied with ARXRD and standard XRD. The diffraction studies yielded information about crystalline species at depths down to approximately 50 nm, 100 nm, 300 nm, 700 nm, and 10 μm.

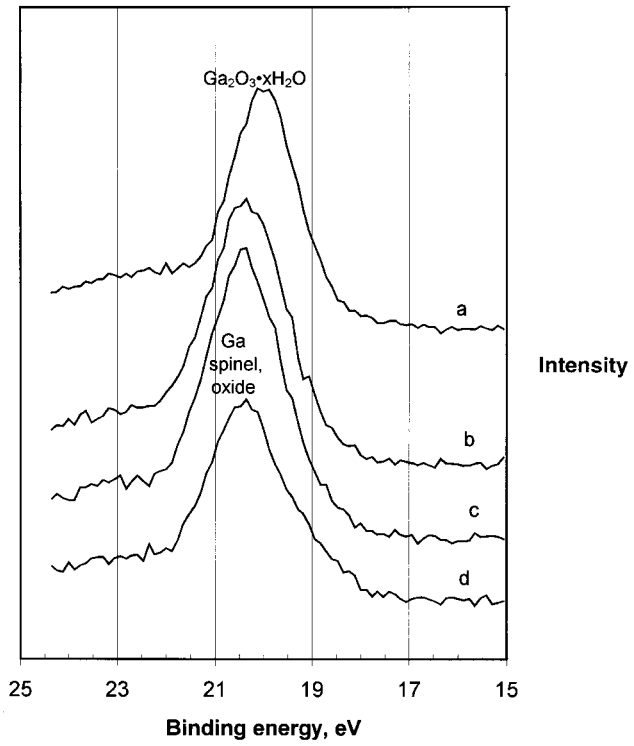

Fig. 1 Oxidized Spartan Plus alloy high resolution x-ray photoelectron spectroscopy of gallium $2p_3$ peaks as a function of argon ion sputtering time (a) as-received surface, (b) 7 min, (c) 25 min, and (d) 200 min. The y-axis is relative intensity and can be correlated to the concentrations given in Table 3.

3. Results

3.1 The Pd-Cu-Ga Spartan Plus Alloy

Table 2 lists one major peak area for each species detected with ARXRD as a function of glancing angle for the oxide of the Spartan Plus material. Table 3 summarizes the atomic percent concentration of elements as a function of depth obtained with XPS. Figures 1 to 3 illustrate the high energy resolution XPS spectra of gallium, copper, and palladium as a function of sputtering time. Similar high resolution spectra were obtained for the balance of the elements detected but are not included for brevity.

Both analyses indicate that the primary component of the oxide layer was actually palladium metal. XRD detected gallium in two phases: βGa_2O_3 and $CuGa_2O_4$, with βGa_2O_3 undetectable at the most shallow glancing angle. With XPS, the main gallium peak detected on the surface of the Spartan Plus oxide occurred at 20.0 eV (Fig. 1). This was presumed to be due to hydrated oxides/hydroxides. With increasing depth, the gallium peak occurred at approximately 20.5 eV, consistent with

gallium oxide. Some gallium metal was also detected. There was no strong peak shift to differentiate the gallium in $CuGa_2O_4$ spinel from the gallium in βGa_2O_3. Additionally, in a mixed component system such as this, XPS would probably be unable to differentiate βGa_2O_3 from αGa_2O_3. XRD indicated copper was also present in two phases, Cu_2O and $CuGa_2O_4$. Rather than the typical XPS peaks used for copper (from the 2p transitions), Auger lines obtained during XPS were used for the analysis of the copper binding energy because Cu^o and Cu_2O cannot be easily differentiated with the 2p peaks. Once again, XPS high resolution peak structure (Fig. 2) showed mixtures of Cu^{2+}, Cu^{1+}, and Cu^o states, shifted slightly due to effects that were presumed to be from the spinel structure. XPS analyses of both copper and palladium compounds are expected to be complicated by differential sputtering effects. Figure 3 shows that the major palladium surface compound is hydrated PdO. With increased sputtering time, the hydrated oxide component decreases in intensity, replaced by increases in the peak for palladium metal. Because PdO is an unstable oxide (Ref 28), it is likely that a fraction of the Pd^o detected is due to sputter reduction. ARXRD also shows an increase in palladium metal with depth.

Neither copper metal, gold, nor gold alloys were detected with x-ray diffraction, but they were detected with XPS at depths of >70 nm. With XPS, gold metal produces a doublet that typically exhibited peaks at 88.0 and 84.0 eV from the $4f_{5/2}$ and $4f_{7/2}$ peaks, respectively. The $4f_{7/2}$ gold peak detected here was shifted to 85.4 eV; this is a relatively large shift for gold (Ref 25). This shift has been correlated to small clusters of metal, of approximately 5 nm, free-standing on substrates and insulating matrices. Although other mechanisms cannot be precluded, an arguable reason for the shift is that gold, as well as perhaps copper, is in an electrically isolated matrix, exhibiting a classic cluster shift (Ref 29). The lack of detection of Au and Cu^o with XRD may be due to microcrystallinity of those species.

The initial ARXRD analysis of the Spartan Plus sample was plagued by a large, unidentifiable peak at $2\theta = 34.6°$. As the angle of incidence increased, the unknown peak decreased in relative intensity. The XPS analysis of the Spartan Plus sample indicated the surface was composed primarily of hydrated oxides, chiefly hydrated palladium oxide (Fig. 3). ICDD states that the major peak for $PdO{\cdot}xH_2O$ is at 34.18°. Conventional XRD analyses of $PdO{\cdot}xH_2O$ and $Pd(OH)_2$ powders (Alfa Aesar, Ward Hill, MA) were conducted; the major peaks occurred at 34.19° and 34.13°, respectively, for those compounds. The peak at 34.6° may be associated with a nonequilibrium form of hydrated palladium oxide or palladium hydroxide, or with stress due to an epitaxial relationship between the palladium oxides or hydroxide and the palladium solid solution matrix in the oxide layer.

The XPS survey scans of the Spartan Plus oxide summarized in Table 3 indicate that the concentration of the layer was not uniform. There are gradual changes in the surface composition, and the data indicate some type of interface was present at the 100 min. sputtering time, corresponding to approximately 70 nm. At this depth, the carbon and gold (microcrystalline form) increased, while the oxygen, gallium, and

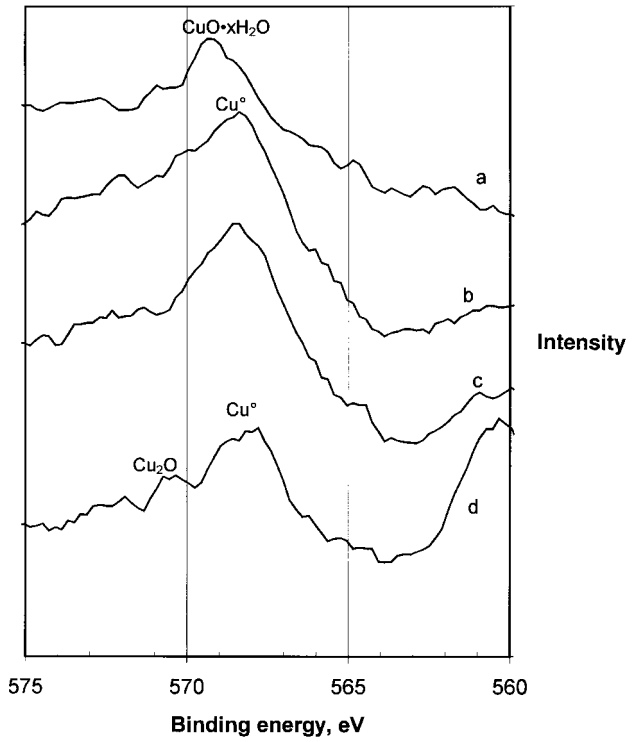

Fig. 2 Oxidized Spartan Plus alloy high resolution x-ray photoelectron spectroscopy of copper LMM Auger transition peaks as a function of argon ion sputtering time (a) as-received surface, (b) 7 min, (c) 25 min, and (d) 200 min

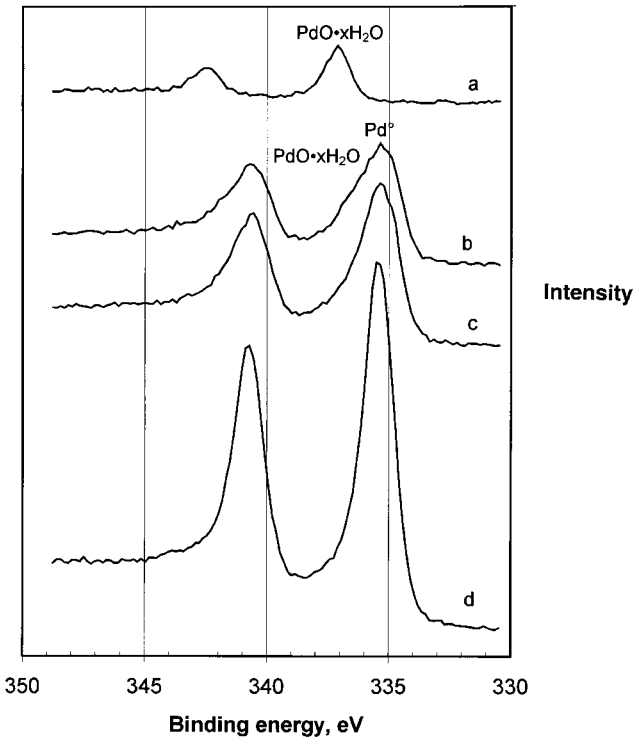

Fig. 3 Oxidized Spartan Plus alloy high resolution x-ray photoelectron spectroscopy of palladium $3d_{5/2}$ peaks as a function of argon ion sputtering time (a) as-received surface, (b) 7 min, (c) 25 min, and (d) 200 min

copper decreased. It is probable that the increased carbon at the 70 nm level is trapped adventitious carbon and that this was the site of an original surface. The copper oxide and spinel grew over the old surface, leaving that original surface somewhat intact. This is also the depth where gold and metallic copper appeared.

3.2 The Pd-Ga Protocol Alloy

Table 4 lists one major peak area for each species detected with ARXRD as a function of glancing angle for the oxidized Protocol sample. Table 5 summarizes the atomic percent concentration of the elements detected as a function of depth obtained with XPS. Figures 4 and 5 illustrate the high energy resolution XPS spectra of gallium and palladium as a function of sputtering time.

The XRD results indicate that the surface again contains substantial palladium metal. With XPS, surface palladium was in the form of PdO (Fig. 5), but the palladium became primarily metallic within 5 nm of the surface. Strong evidence of hydrated palladium oxide was not detected with XPS, and the XRD peak at 34.6° was also not present. ARXRD verified an

Table 4 Peaks areas (arbitrary units) as a function of glancing angle for oxidized Protocol alloy

			ARXRD method, incident angle				Standard XRD
	ICDD file no.	Peak location, 2θ	0.75°	1.5°	5°	20°	method
Pd	5-681	40.1	848	2 324	8 652	32 379	31 220
PdO	41-1107	33.9	50	129	309	483	437
In_2O_3	6-416	30.6	34	79	316	622	431
βGa_2O_3	43-1012	31.7	67	146	451	809	898

Table 5 Elemental concentration (at.%) obtained by XPS as a function of sputtering time for oxidized Protocol alloy

Argon ion sputtering time, min	C 1s	O 1s	S 2p	Ga $2p_3$	Pd $3d_{5/2}$	Ag $3d_{5/2}$	In $3d_{5/2}$	Au $4f_{7/2}$
0	27.3	50.2	1.0	10.7	6.0	1.3	3.2	0.2
1	17.5	55.6	1.2	14.4	6.9	1.1	3.0	0.4
3	16.5	53.8	1.4	15.5	9.0	0.9	2.5	0.3
7	11.7	56.3	1.5	16.9	10.4	0.7	2.1	0.4
15	11.4	53.8	1.7	18.3	11.3	1.1	1.7	0.7
25	8.6	55.6	1.8	18.1	12.2	1.2	1.8	0.7
100	7.9	53.2	1.6	18.4	14.7	1.7	1.4	1.1
200	6.7	54.6	1.5	19.5	14.2	1.4	1.1	1.0
300	5.1	55.6	1.5	21.7	12.7	1.4	1.1	0.9

Table 6 Peak areas (arbitrary units) as a function of glancing angle for oxidized Legacy alloy

			ARXRD method, incident angle				Standard XRD
	ICDD file no.	Peak location, 2θ	0.75°	1.5°	5°	20°	method
Pd	5-681	40.1	1 298	2 848	9 559	30 773	28 799
PdO	41-1107	33.9	91	162	450	1 030	995
βGa_2O_3	43-1012	31.7	25	45	156	300	326
Ga	27-0222	36.3	13	0	36	255	780

Table 7 Elemental concentration (at.%) obtained by XPS as a function of sputtering time for oxidized Legacy alloy

Argon ion sputtering time, min	C 1s	O 1s	Ga $2p_3$	Pd $3d_{5/2}$	Ag $3d_{5/2}$	In $3d_{5/2}$	Au $4f_{7/2}$
0	41.3	42.8	4.8	9.7	0.4	0.7	0.3
1	26.5	43.6	8.8	19.8	0.3	0.5	0.5
3	24.3	42.7	8.5	23.3	0.3	0.4	0.5
7	19.5	44.2	8.9	26.0	0.4	0.4	0.6
15	21.2	42.5	9.4	25.6	0.3	0.4	0.5
25	18.2	42.8	9.9	27.8	0.3	0.4	0.6
100	16.6	41.0	9.7	31.3	0.2	0.4	0.7
200	15.2	41.7	9.8	31.9	0.3	0.4	0.7
300	14.5	42.0	10.3	31.7	0.3	0.4	0.7

increase in Pd° with depth. Sulfur, silver, indium, and gold were detected with XPS in the outer 200 nm, but the major components were consistent with elevated gallium and oxygen. Not in the nominal alloy composition, sulfur was presumed to be a contaminant. The XPS results indicate that the surface contained hydrated gallium oxide, while the immediate subsurface depths contain anhydrous gallium oxide (Fig. 4). Both ARXRD and conventional XRD established that this oxide was relatively uniform βGa_2O_3. Unless the processing conditions are such that some internal hydration is induced (as in the case of the Spartan Plus alloy), air-induced aquation occurs near the outer surface and does not affect subsurface metallic species. Carbon was relatively high in concentration and slowly decreased throughout the thickness analyzed.

3.3 The Pd-Ga Legacy Alloy

Table 6 lists one peak area for each species detected with ARXRD as a function of glancing angle for the oxidized surface of the Legacy alloy. Table 7 summarizes the atomic percent concentration of elements as a function of depth obtained with XPS. Figures 6 and 7 illustrate the high energy resolution XPS spectra of gallium and palladium as a function of sputtering time.

The results indicate that the coating on the Legacy sample is primarily palladium metal, PdO, βGa_2O_3, and perhaps metallic gallium. According to the XPS results, gallium metal, gallium oxide, and hydrated gallium oxide were present at the surface (Fig. 6). In_2O_3, gold, and silver were also detected. Surface palladium was in the form of Pd metal and some hydrated PdO, but the palladium became primarily metallic in form within 5 nm of the surface (Fig. 7). Consistently, XRD analysis indicated that the peak at 34.6°, which is hypothesized to be nonequili-

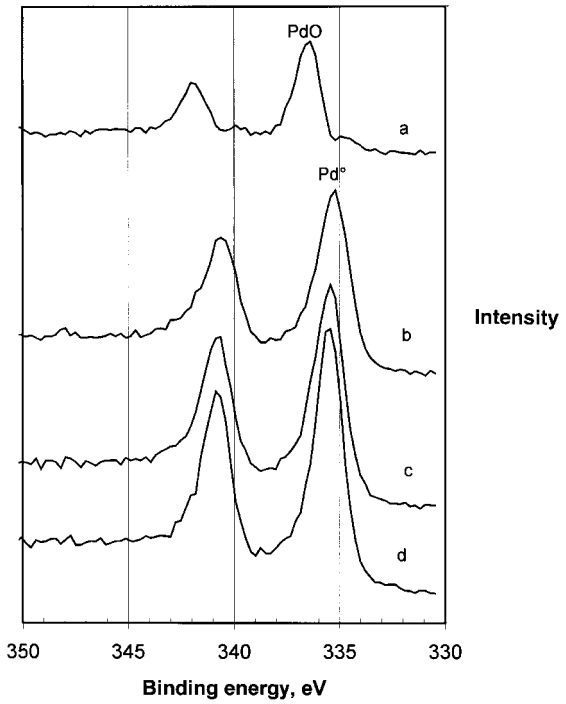

Fig. 5 Oxidized Protocol alloy high resolution x-ray photoelectron spectroscopy of palladium $3d_{5/2}$ peaks as a function of argon ion sputtering time (a) as-received surface, (b) 7 min, (c) 25 min, and (d) 200 min

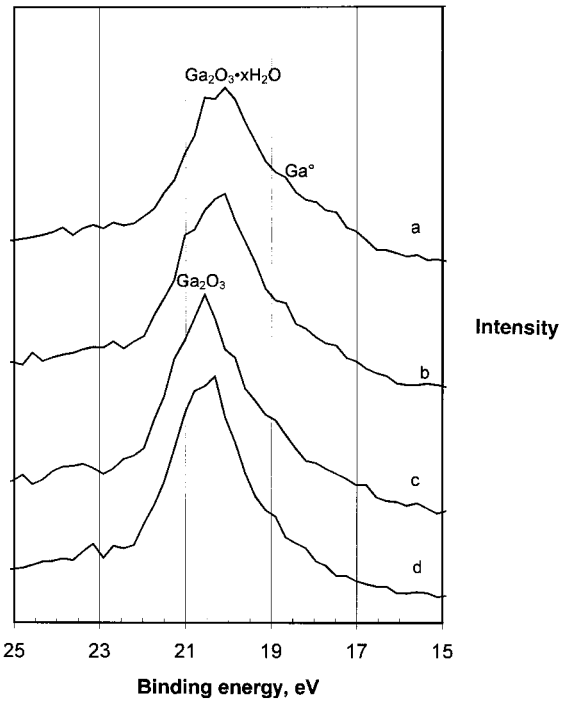

Fig. 4 Oxidized Protocol alloy high resolution x-ray photoelectron spectroscopy of gallium $2p_3$ peaks as a function of argon ion sputtering time (a) as-received surface, (b) 7 min, (c) 25 min, and (d) 200 min

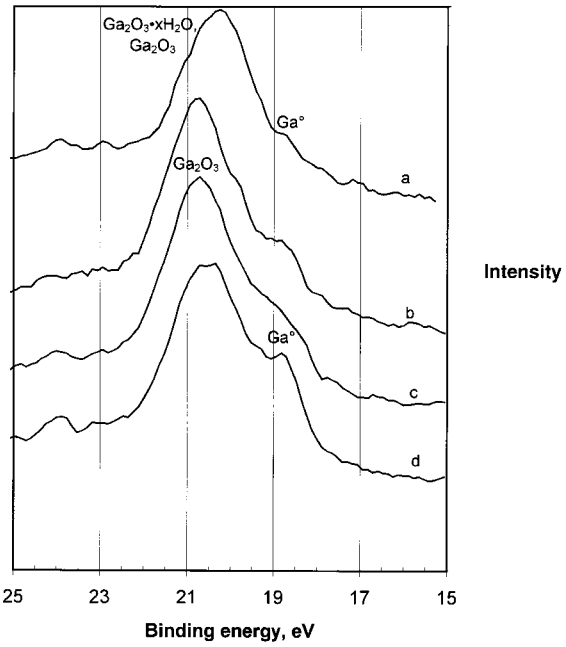

Fig. 6 Oxidized Legacy alloy high resolution x-ray photoelectron spectroscopy of gallium $2p_3$ peaks as a function of argon ion sputtering time (a) as-received surface, (b) 7 min, (c) 25 min, and (d) 200 min

brium $PdO \cdot xH_2O$ or $Pd(OH)_2$, was not present. Once again, XPS indicated that carbon was relatively high in concentration at the surface and slowly decreased throughout the thickness analyzed.

Figure 8 presents a narrow 2θ range of the ARXRD plots as a function of the angle of incidence. It illustrates the increased presence of gallium oxides as a function of depth, consistent with the XPS results. Additionally, the presence of metallic gallium (ICDD standard 27-222) is suggested by the peak at 36.2° on the 5° and 20° incident angle scans; very small peaks may exist on the 0.75° and 1.5° scans. The other strong peaks for metallic gallium may be obscured by more intense overlapping peaks from PdO and βGa_2O_3 or diminished in intensity due to preferred orientation. Moreover, this peak at 36.2° does not match the ICDD standard (43-1012) for βGa_2O_3 and was not reported previously (Ref 18) on the conventional x-ray diffraction analyses of these high-palladium alloys. While it seems that the oxide layer on this alloy should not contain substantial quantities of metallic gallium, an alternative interpretation has not been found. Figure 6 also shows consistent metallic gallium with sputtering time. It is not believed that the gallium metal detected with XPS is due to sputter reduction of gallium oxide because it is present on the before-sputtered surface and because gallium oxide is a relatively stable oxide.

The Legacy alloy also exhibits a slightly different palladium metal XRD profile compared to the other two alloys in that the 10 μm depth appears to have somewhat less Pd metal (relative to the other alloys) than the 700 nm depth. In the other alloys, the relative palladium metal concentration always increased with increasing depth.

4. Discussion

For these dental alloys, sputtering with Ar^+ during XPS depth profiling may induce, to some degree, the following reactions:

$$PdO \rightarrow 2Pd + O_2\uparrow$$

$$2CuO \rightarrow Cu_2O + \tfrac{1}{2}O_2\uparrow$$

$CuGa_2O_4 \rightarrow 2CuO$ (further reduces to Cu_2O as shown above) + Ga_2O_3 (stable)

$$In_2O_3 \rightarrow \text{Stable}$$

Although it is often possible to interpret data based upon these anticipated reactions, the combined use of XPS and XRD was extremely beneficial in the identification of near-surface species. The terminology of angle-resolved x-ray diffraction, rather than the conventional grazing-angle x-ray diffraction (GXRD), has been adopted because some of the incident angles used were much greater than that typically called grazing. The present terminology was chosen because of its correspondence to the familiar use of angle-resolved XPS for the depth profiling of thin surface layers (Ref 13).

Oxide scales can grow by two mechanisms. The oxygen (or oxygen ion) can diffuse through the scale to the metal, causing the scale to grow at the metal-oxide interface. The second possibility is that the metal (or metal ion) can diffuse through the scale to the surface and react with oxygen, causing the scale to grow at the oxide-air interface (Ref 30). The data indicate that

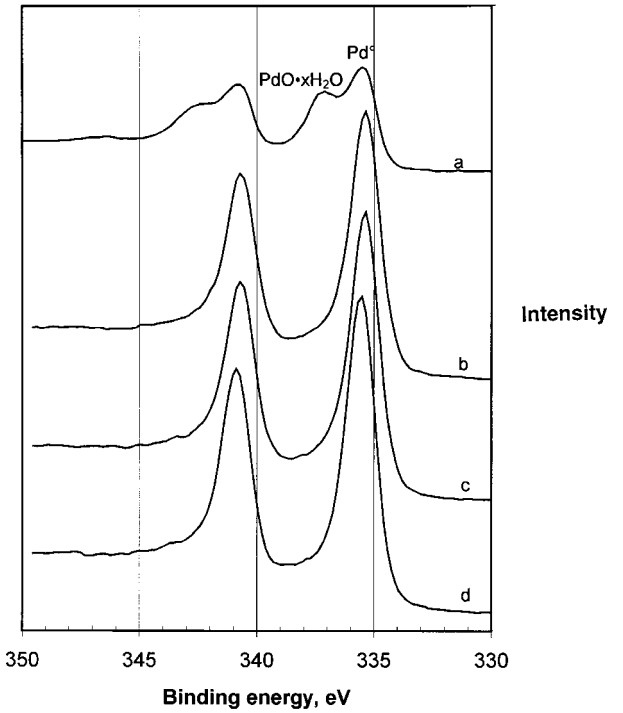

Fig. 7 Oxidized Legacy alloy high resolution x-ray photoelectron spectroscopy of palladium as a function of argon ion sputtering time (a) as-received surface, (b) 7 min, (c) 25 min, and (d) 200 min

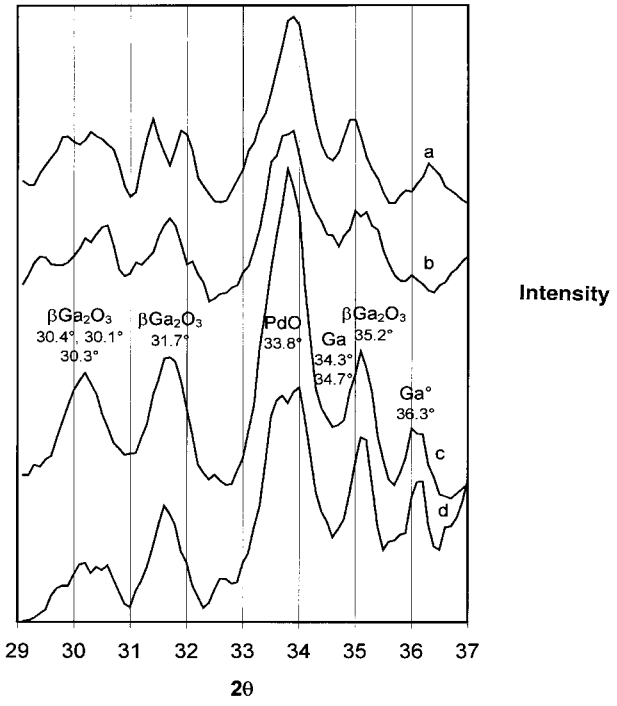

Fig. 8 Angle-resolved x-ray diffraction of oxidized Legacy alloy. Scan *a* is incident angle α = 0.75°; scan *b* is incident angle α = 1.5°; scan *c* is incident angle α = 5°; scan *d* is incident angle α = 20°.

the second scenario occurred in the oxidation of the Spartan Plus alloy. The gold and copper microcrystals may be present in the cast material, and the layer from 0 to 70 nm deep is the new oxide that grew up over these microcrystals, the base material, and the original adventitious carbon. Hydrated palladium oxide, detected with both techniques, was present to a substantial depth because fresh PdO kept forming at the surface and reacting with the oxidation atmosphere, including some water vapor.

In contrast, the data seem to indicate that the oxide layers on the Pd-Ga alloys (Protocol and Legacy) are each grown by oxygen (or oxygen ions) diffusing through the scale to the metal, causing the scale to grow at the metal-oxide interface. This is the opposite mechanism to that theorized for Pd-Cu-Ga alloy (Spartan Plus). The uniform oxygen concentrations summarized in Tables 5 and 7 help to substantiate this point. Hydrated palladium oxide was not detected to any substantial degree in the bulk of these oxides for the Protocol and Legacy samples because there was no continually generated fresh PdO surface for reaction. Thus, once the surface hydrated layer was formed, that reaction was complete. Additionally, there was incomplete oxidation of some of the elements in the Legacy and Protocol oxide layers, that is, both indium and gallium showed signs of significant metallic species inside the Protocol layer, and gallium metal was present in the Legacy layer.

These contrasting layer growth mechanisms may also account for the detected differences in oxide layer adhesion. The oxide layer on the Protocol and Legacy samples could be expected to be less adherent to its substrate than for the Spartan Plus alloy because the layer growth at the metal-oxide interface on the Protocol and Legacy samples would yield a more distinct transition and have a poorer epitaxial match than the more gradual layer grown on the surface of the Spartan Plus sample. These features were found to be the case during porcelain adherence testing. The Pd-Ga alloys, Protocol and Legacy, exhibited substantial or complete fracture through the metal-oxide interface. The mechanism of the layer growth undoubtedly played a role in the weakness of the oxide layer adhesion.

5. Conclusions

The combined use of XPS and ARXRD is an effective method for studying complex oxide layers on multicomponent Pd-Ga based dental alloys. The techniques were mutually beneficial in identifying features that did not correlate to published standards. The experiments helped to hypothesize the mechanism of oxide layer growth. The oxide layer on the Spartan Plus Pd-Cu-Ga alloy was determined to grow primarily via metal, or metal ions, diffusing through the scale to the surface and reacting with oxygen, causing the scale to grow at the oxide-air interface. In contrast, the oxide layer on the Protocol and Legacy Pd-Ga samples was formed primarily by oxygen, or oxygen ions, diffusing through the scale to the metal, causing the scale to grow at the metal-oxide interface. These opposing mechanisms may be correlated to the ultimate adhesion of the oxide layer upon mechanical testing. XPS, combined with depth profiling, provides information from the surface to subsurface, while ARXRD profiles from the subsurface to the bulk.

Acknowledgments

Support for this investigation was received from research grant DE10147 from the National Institute of Dental Research, Bethesda, MD. The authors wish to thank Professor Rodney Tettenhorst, Department of Geological Sciences, The Ohio State University, for the use of his x-ray diffractometer to investigate the palladium oxides and hydroxide.

References

1. L.D. Madsen and L. Weaver, Examination of Titanium Oxides, Lead Oxides, and Lead Titanates using X-Ray Diffraction and Raman Spectroscopy, *Mater. Res. Soc. Symp. Proc.*, Vol 310, 1993, p 385-390
2. A.Z. Moshfegh and A. Ignatiev, Formation and Characterization of Thin-Film Vanadium Oxides: Auger Electron Spectroscopy, X-Ray Photoelectron Spectroscopy, X-Ray Diffraction, Scanning Electron Microscopy, and Optical Reflectance Studies, *Thin Solid Films*, Vol 198 (No. 1 and 2), 1991, p 251-268
3. C. Onneby and C.G. Pantano, Silicon Oxycarbide Formation on SiC Surfaces and at the SiC/SiO_2 Interface, *J. Vac. Sci. Technol.*, A, Vol 15 (No. 3), 1997, p 1597-1602
4. S.W. Gaarenstroom, Growth and Characterization of Aluminum Oxide Thin Films for Evaluation as Reference Materials, *J. Vac. Sci. Technol.*, A, Vol 15, 1997, p 470-477
5. M.N. Islam, T.B. Ghosh, K.L. Chopra, and H.N. Acharya, XPS and X-Ray Diffraction Studies of Aluminum-Doped Zinc Oxide Transparent Conducting Films, *Thin Solid Films*, Vol 280, 1996, p 20-25
6. K. Asami and K. Hashimoto, The X-Ray Photoelectron Spectra of Several Oxides of Iron and Chromium, *Corros. Sci.*, Vol 17, 1977, p 559-570
7. R.P. Goehner and M.O. Eatough, A Study of Grazing Incidence Configurations and Their Effect on X-Ray Diffraction Data, *Powder Diffr.*, Vol 7, 1992, p 2-5
8. M. Brunel and F. DeBergevin, X-Ray Beam Diffraction at Grazing Incidence, *Acta Crystallogr.*, Vol A42, 1986, p 299-303 (in French)
9. D.G. Neerinck and T.J. Vink, Depth Profiling of Thin ITO Films by Grazing Incidence X-Ray Diffraction, *Thin Solid Films*, Vol 278, 1996, p 12-17
10. M.F. Toney and T.C. Huang, X-Ray Depth Profiling of Iron Oxide Thin Films, *J. Mater. Res.*, Vol 3, 1988, p 351-356
11. R.P. Goehner, M.O. Eatough, B.A. Tuttle, and T.J. Headley, *Adv. in X-Ray Analysis*, Vol 35, 1992, p 159-167
12. F. Pons, S. Megtert, J.C. Pivin, M. Pequignot, D. Mairey, and C. Roques-Carmes, Application of a Grazing-Incidence X-Ray Diffraction Technique to the Depth-Resolved Analysis of Structural Transformations due to Surface Treatment, *J. Appl. Crystallogr.*, Vol 21, 1988, p 197-205
13. C.S. Fadley, Angle-Resolved X-Ray Photoelectron Spectroscopy, *Prog. Surf. Sci.*, Vol 16, 1984, p 275-388
14. S.J. Kerber, T.L. Barr, G.P. Mann, W.A. Brantley, E. Papazoglou, and J.C. Mitchell, The Complementary Nature of X-Ray Photoelectron Spectroscopy and Angle-Resolved X-Ray Diffraction—Part I: Background and Theory, *J. Mater. Eng. Perform.*, Vol 7 (No. 3), 1998, p 329-333
15. W.A. Brantley, Z. Cai, A.B. Carr, and J.C. Mitchell, Metallurgical Structures of As-Cast and Heat-Treated High-Palladium Dental Alloys, *Cells and Mater.*, Vol 3, 1993, p 103-114
16. A.B. Carr and W.A. Brantley, New High-Palladium Casting Alloys: Part 1, Overview and Initial Studies, *Int. J. Prosthodont*, Vol 4, 1991, p 265-275
17. J.A. Hautaniemi, J.T. Juhanoja, E.J. Suoninen, and A.U.O. Yli-Urpo, Oxidation of Four Palladium-Rich Ceramic Fusing Alloys, *Biomater.*, Vol 11, 1990, p 62-72

18. W.A. Brantley, Z. Cai, E. Papazoglou, J.C. Mitchell, S.J. Kerber, G.P. Mann, and T.L. Barr, X-Ray Diffraction Studies of Oxidized High-Palladium Alloys, *Dent. Mater.*, Vol 12, 1996, p 333-341

19. E. Papazoglou, W.A. Brantley, A.B. Carr, and W.M. Johnston, Porcelain Adherence to High-Palladium Alloys, *J. Prosthet. Dent.*, Vol 70, 1993, p 386-394

20. S. Kerber, G. Mann, T. Barr, W. Brantley, and E. Papazoglou, X-Ray Photoelectron Spectroscopic Analysis of an Oxidized Pd-Cu-Ga Alloy, *J. Dent. Res.*, Vol 76 (Special Issue), 1997, p 402

21. A.B. Carr, Z. Cai, W.A. Brantley, and J.C. Mitchell, New High-Palladium Casting Alloys: Part 2, Effects of Heat Treatment and Burnout Temperature, *Int. J. Prosthodont*, Vol 6, 1993, p 233-241

22. L.V. Azároff, *Elements of X-Ray Crystallography*, McGraw-Hill Book Co., 1968, p 549

23. B.D. Cullity, *Elements of X-Ray Diffraction*, 2nd ed., Addison-Wesley, 1978, p 188

24. C.D. Wagner, *Practical Surface Analysis by Auger and X-Ray Photoelectron Spectroscopy*, D. Briggs and M.P. Seah, Ed., John Wiley & Sons, 1983, p 477-509

25. J.F. Moulder, W.F. Stickle, P.E. Sobol, and K.D. Bomben, *Handbook of X-Ray Photoelectron Spectroscopy*, Physical Electronics, Inc., 1995

26. T.L. Barr, *Modern ESCA*, CRC Press, 1994, p 339

27. C.D. Wagner, *Practical Surface Analysis by Auger and X-Ray Photoelectron Spectroscopy*, D. Briggs and M.P. Seah, Ed., John Wiley & Sons, 1983, p 511-514

28. K.S. Kim, W.E. Baitinger, J.W. Amy, and N. Winograd, ESCA Studies of Metal-Oxygen Surfaces using Argon and Oxygen Ion-Bombardment, *J. Electron Spectrosc. Relat. Phenom.*, Vol 4, 1974, p 351-367

29. T.L. Barr, *Modern ESCA*, CRC Press, 1994, p 310-312

30. J.T.N. Atkinson and H. VanDroffelaar, *Corrosion and Its Control*, National Association of Corrosion Engineers, Houston, 1982, p 43